Available online at www.sciencedirect.com
ScienceDirect
Engineering Fracture Mechanics 75 (2008) 3101–3120
Engineering Fracture Mechanics
www.elsevier.com/locate/engfracmech

Numerical simulation of plasticity induced crack closure: Identification and discussion of parameters

F.V. Antunes *, D.M. Rodrigues

Department of Mechanical Engineering, Faculty of Science and Technology, University of Coimbra, Pinhal de Marrocos, 3030-788 Coimbra, Portugal

Received 23 October 2006; received in revised form 15 November 2007; accepted 17 December 2007
Available online 28 December 2007

Abstract

Numerical studies play a major role in the understanding and prediction of plasticity induced crack closure (PICC). However, the available numerical models can be considered simplifications of reality as they consider discrete crack propagations, relatively high fatigue crack growth rates (FCGR), sharp cracks, and propagation occurring at well-defined loads. Besides, there are a great number of numerical and physical parameters affecting the predictions of PICC. The aim of this paper is to discuss the numerical study of PICC. The numerical parameters affecting the accuracy of the numerical simulations, and the dependent parameters used to characterise the plastic wake and the closure level, are identified. The influence of the radial size of crack front elements and crack propagation is analysed. An extrapolation model is proposed, with excellent results. An intrinsic uncertainty is associated with the number of load cycles between crack increments and the definition of crack closure level. Finally, the effect of the stress ratio (R) on crack closure level is analysed.

Keywords: Plasticity induced crack closure; Finite element analysis; Middle-crack tension specimen; Elastic–plastic material behaviour; Numerical parameters

1. Introduction

Crack closure is a phenomenon that consists of the contact between fracture surfaces during a portion of the load cycle. This contact affects the local stress and plastic deformation fields near the crack tip, and thus the micro mechanisms responsible for fatigue propagation (cyclic plastic deformation, oxidation, creep, etc.). Crack closure is able to explain the influence of mean stress in both regimes I and II of crack propagation [1,2], and transient crack growth behaviour following overloads [3], among other aspects, must therefore be considered in the design of components.

* Corresponding author. Tel.: +351 239 790722; fax: +351 239 790701.
E-mail address: fernando.ventura@dem.uc.pt (F.V. Antunes).

0013-7944/$ - see front matter © 2007 Elsevier Ltd. All rights reserved.
doi:10.1016/j.engfracmech.2007.12.009

The idea that fracture surface interaction leads to a decrease in stress intensity at the crack tip and to an increase in fatigue life was proposed in 1963 [4]. Elber [1,5] discussed the concept in terms of fracture mechanics parameters, promoting a strong research effort into the mechanisms and phenomena associated with fatigue crack closure [6]. Ritchie et al. [7] and Suresh [8,9] identified the main closure mechanisms, which are plasticity induced crack closure (PICC), oxide induced crack closure and roughness induced crack closure. Additional mechanisms, such as viscous-fluid induced crack closure [10], transformation-induced crack closure [11] and graphite induced crack closure [12], have been observed to operate in susceptible materials and environments.

While some researchers argue that PICC does not exist (particularly for plain strain conditions) [13–15], a huge amount of experimental, numerical and analytical work has been performed, supporting the existence of crack closure and its influence on fatigue crack propagation. Various methods have been employed to measure crack opening and crack closure levels experimentally [16], however these only give average values, therefore numerical approaches become fundamental tools for studying crack closure, specially along 3D crack fronts. Furthermore, once a numerical procedure has been optimised, it is relatively simple to adapt it to new load conditions, materials, crack lengths, etc. Nevertheless, the finite element models must be correctly defined and their limitations understood. The numerical simulation of PICC is still complicated due to the difficulties in modelling complex material behaviour, contact between crack faces during crack closure and crack propagation. These complexities, and the large number of numerical and physical independent parameters affecting PICC, to some degree explain contradictory literature results. Despite their limitations, existing numerical models are useful for improving the understanding of the influence of different physical parameters like thickness, stress ratio or overload ratio on closure behaviour. Further study is required to fully understand the effect of the finite element mesh and of the number of load cycles between crack increments, and to establish parameters which can quantify the influence of closure on fatigue crack growth. Considering the vast parametric space in question, general conclusions are always subject to uncertainty, therefore each practical situation must be carefully analysed to ensure feasible results.

The main objective of this paper is to discuss the numerical study of PICC, namely, the numerical parameters affecting the results of the numerical simulations, and the dependent parameters used to characterise plastic wake and closure level. Afterwards, the intrinsic uncertainty of the numerical predictions is studied by analysing the influence of the closure definition and the number of load cycles between increments on crack closure level. Finally, the influence of stress ratio ($\sigma_{min}/\sigma_{max}$) on crack closure is studied.

2. Overview on physical and numerical parameters affecting PICC

2.1. Physical aspects

There are several models that try to relate the occurrence of cyclic plastic deformation at the crack tip to crack propagation and the formation of striations usually observed on the fracture surface of ductile materials. All the models are based on the fact that the fatigue crack propagation process is repetitive, so each of them tries to explain the mechanism of crack propagation by explaining the process that happens during a single load cycle [17].

Laird's model of striation formation by crack tip plastic blunting [18,19] is largely accepted as a general description of the propagation mechanism of fatigue cracks in regime II of da/dN–ΔK curves. According to this model, plastic deformation at the crack tip is highly concentrated at 45°, producing blunting and creation of new fracture surfaces. When the stress reverses during load cycles, crack tip compression stresses reverse slipping, the fracture surfaces approach, but the new surface cannot be removed by reconnection of the atomic bonds, which is in accordance with the entropy law of thermodynamics. Other mechanisms exist that explain propagation at relatively low stress amplitudes (cleavage) and at relatively high stress amplitudes (coalescence of microvoids, etc.). At elevated temperatures, diffusion based mechanisms, like oxidation and creep, may become dominant.

As the crack propagates due to cyclic loading, a residual plastic wake is formed. The deformed material acts as a wedge behind the crack tip and the contact between fracture surfaces is induced by the elastically

deformed remote material. This mechanism affects the fatigue crack propagation rate and is known as plasticity induced crack closure, as previously noted. Under plane stress conditions, i.e., near the surface, this phenomenon happens due to the transportation of material to the interior of the sub-surface region.

2.2. Numerical aspects

The numerical analysis of PICC based on finite element method (FEM) consists of discretising and modelling the cracked body having elastic–plastic behaviour, applying a cyclic load, extending the crack and measuring the crack closure level. The finite element mesh must be highly refined near the crack front, with radial sizes (L_1) at the micron scale, in order to model the forward and reversed crack tip plastic zones. The forward plastic zone is made up of the material near the crack tip undergoing plastic deformation at the maximum load, therefore it is intimately related to K_{max}. The reversed plastic zone encompasses the material near the crack tip undergoing compressive yielding at the minimum load and is related to ΔK.

Commercial FE software packages offer tools to deal with elastic–plastic deformation, crack propagation and contact between crack flanks, and are therefore adequate to model PICC. However, the numerical models have significant simplifications with respect to real fatigue crack propagation, namely:

- discrete crack propagations, of the same size as near crack tip elements, which give fatigue crack growth rates significantly higher than real values;
- crack propagation is modelled at a constant load when in reality it occurs continuously during the whole load cycle;
- relatively low FCGR, which affects the number of load cycles applied to each near crack tip point. This error can be reduced by decreasing L_1 and increasing the number of load cycles between propagations;
- crack tip shape. Sharp cracks are usually modelled, however, real cracks have a non-zero radius at the tip, within micron range, which affects the local plastic deformation fields. Despite all efforts to improve the accuracy of the numerical predictions, the crack tip results will always be affected by significant numerical errors due to the local singularity;
- elastic–plastic behaviour is seldom well modelled. The cyclic plastic deformation of material near the crack tip involving strain ratcheting, stress relaxation and cyclic hardening or softening is difficult to model, and the material models and material constants available are in general quite limited.

Additionally, numerical models are usually aseptic, since they only simulate PICC, neglecting all other phenomena that may exist, like roughness induced or oxide induced crack closure. Therefore, comparison of numerical and experimental results, which may include these additional mechanisms, must be done carefully. Besides, it is not clear how global closure measurements obtained experimentally should be compared to punctual values given by the first node contact, stress inversion or other closure definitions.

Considering all the previous aspects, despite the great number of studies on PICC there is still a lack of confidence in the numerical predictions. Further study is still required to optimise the numerical parameters for a wide range of physical variables and to establish closure parameters adequate to quantify its influence on fatigue crack growth. The numerical parameters that have to be optimized, which can be arbitrarily selected by the researcher, are associated with:

1. finite element discretisation,
2. the crack propagation scheme,
3. the closure definition, and
4. the material model.

The literature references, in both Tables 1 and 2, indicate studies focused on the different parameters. As can be seen, there is a huge parametric space. In order to reduce the parametric space, several options are usually chosen at the beginning of model definition, considering previous results from the literature and the previous experience of the authors. As indicated in Table 2, significant work has been developed to optimize the

Table 1
Independent physical parameters

Material	Homogeneity and isotropy Elastic and plastic behaviour Fatigue behaviour
Sample geometry	Thickness [21,23] Crack length (a or a/W) [24–28] Crack shape [29]
Loading parameters	Loading mode (modes I, II or III, mixed mode, multiaxial loading) $\Delta\sigma/\sigma_{ys}$ σ_{max}/σ_{ys} Mean stress (normally quantified by the cyclic stress ratio, $R = \sigma_{min}/\sigma_{max}$) Load history (constant amplitude, overloads, blocks, random load) [20,29–31]

Table 2
Independent numerical parameters

Material model	Yield criterium Flow rule Hardening laws (kinematic and/or isotropic) [20,21,23,30,32–36]
Numerical simulation program	Time integration strategy Parameters of the numerical algorithm
Mesh	Type of element and integration Radial size of crack front elements (L_1 or L_1/r_p) [21,23,24,28,35–38] Mesh refinement along crack front Mesh remote from crack front
Crack propagation scheme	Propagation at maximum, minimum or intermediate load [24,28,38–42] Extent of individual crack increments ($\Delta a = \text{constant} \times L_1$) [43] Number of load cycles between crack increments ($\geqslant 2$) [35] Number of crack increments necessary for stabilisation ($\Delta a = \Sigma\Delta a_i \geqslant r_{p,m}$) [21,28,35,37]
Closure definition	Last contact or inversion of stresses at crack tip [22,44] Crack opening or crack closure [36,45]

numerical parameters and relevant conclusions have been found. Revision papers have been published by McClung and Sehitoglu [42], Solanki et al. [46] and Jiang et al. [35], among others.

2.2.1. Finite element discretization

The crack tip is a zone with severe gradients of stress and strain therefore the type and radial size of finite elements are its main parameters. There is a general agreement on the use of a regular mesh with linear or quadratic square elements. On the other hand, the influence of the radial size of crack front elements (L_1) on crack closure is still unclear. Classical mesh refinement studies have been developed, however the literature disagrees about the existence of the typical convergence of results with mesh refinement. Gonzalez and Zapatero [36] considered up to 140 linear elements within the monotonous plastic zone and found near stable closure values. Parks et al. [38] considered a pure kinematic hardening model and obtained a minimum stable value of U for $L_1/r_{p,c} \approx 0.77$–0.91, the size of the cyclic plastic zone being $r_{p,c}$.

The finite element mesh must be sufficiently refined in order to enable the simulation of the plastic deformation phenomena occurring at the crack tip, namely, the formation of the forward and reversed plastic zones. Since the reversed zone is smaller than the forward zone, its size is critical for the definition of L_1. According to Solancki et al. [28], there must be 3–4 linear elements within the reversed plastic zone, while Roychowdhury and Dodds [21] suggested 2–3 linear elements. Solanki et al. [28] indicated that a crack growing under cyclic loading with $R = 0$ had a reversed plastic zone about 1/10 the size of the forward plastic zone (while for a stationary crack this is about 1/4 the size). Therefore, if L_1 is too large, the occurrence

of reversed plasticity will not be modelled. The increase in ΔK, produced by the increase in crack length or $\Delta\sigma$, and the use of higher order elements may be accomplished by an increase in L_1. The increase in stress ratio (R) reduces the size of the reversed plastic zone, and therefore, the use of a finer mesh must be considered.

Additionally, as already stated, the reduction of L_1 brings numerical models closer to real fatigue crack propagation rates, as it reduces the individual crack increment size and increases the number of load cycles applied to each near crack tip point. However, decreasing L_1 substantially increases the numerical effort, by decreasing the size of individual crack increment, Δa_i, and the total number of finite elements within the model. These determine the computation time (quite high in elastic–plastic analysis) and disk space requirements. According Jiang et al. [35], a lower boundary for L_1 is 0.001 mm. The mesh refinement also affects the position of the first node behind crack tip, which significantly influences the opening level as discussed in point 4.5.

It is also important to note that the most refined mesh area has to include the entire crack tip plastic zone, i.e., the plastic region cannot extend to the transition mesh [46]. Transition region size ratios less than 3 are needed for the mesh [28]. The remote mesh must be quite large to reduce the numerical effort to acceptable levels.

2.2.2. Crack propagation scheme

During numerical simulations the crack can be incremented at maximum load [47], at minimum load [30,39] or at other positions of the load cycle. Ogura et al. [40] advanced the crack when the crack tip reaction force reached zero during the load cycle. However, none of these approaches truly represents the fatigue process, where, according to slip models of striation formation, crack extension is a progressive process occurring during the entire load cycle. The proposal to increment at minimum load was designed to overcome convergence difficulties caused by propagating the crack at maximum load. This is an unrealistic option since the crack is not expected to propagate in a compressive stress field. However, several authors [28,28,42] have already found that the load at which the crack increment occurs does not significantly influence crack closure numerical results.

Under constant amplitude loading, crack tip opening load will typically increase monotonically, with increasing crack growth, until a stabilized value is reached. So, it is important to define the minimum crack extension needed to stabilize the opening level. It is usually sufficient to increase the crack ahead of the monotonic plastic zone resulting from the first load cycle [38,43,48].

2.2.3. Closure definition

A major aspect in the numerical study of PICC is the concept of crack closure. Different concepts have been considered, namely [49]:

- the first contact of crack flank, which corresponds to the contact of the first node behind the current crack tip. This is the conventional definition proposed by Elber [3] and has been widely used [35, etc.]. However, results are mesh-dependent, since the proximity of the first node to the crack tip increases the opening load;
- the first contact of other nodes behind the crack tip. Pommier [30] and Roychowdhury and Dodds [21] considered the second node behind the crack tip;
- the occurrence of compressive stresses at the crack tip [50]. Important differences in crack closure levels are apparent when comparing the classical definition with stress inversion [22,50,51];
- parameters based on remote measurements of displacements or strains, replicating experimental measurements [3];
- a load corresponding to a zero stress intensity factor. Shterenlikht et al. [52] applied optical techniques to determine the stress intensity factor and considered that crack closure occurs when $K = 0$;
- the stress intensity factor required to open the crack, computed using the contact stresses along the closed or partially closed crack under minimum load [44]. The contact stress method overcomes the limitation of focusing attention on a single node, considering instead the global behaviour of the entire crack surface.

Table 3
Dependent parameters for closure characterisation

Parameter	Description	Comment
$r_{c,y}$, $r_{c,x}$, $r_{c,max}$	Extension of reversed plastic zone	Plastic deformation parameters
$r_{p,y}$, $r_{p,x}$, $r_{p,max}$	Extension of monotonic plastic zone (Fig. 2)	
$\bar{\varepsilon}^p = \bar{\varepsilon}^p(x)$	Plastic deformation field	
$d\bar{\varepsilon}^p_B/dx$	Gradient of plastic deformation	
	Cumulative plastic strain energy density	
$\sigma_{residual}(x)/\sigma_{ys}$	Residual stress field near crack tip	Stress fields
$\sigma = \bar{f}(\bar{\varepsilon})$	Stress–strain curve	
	Contact forces at minimum load	Local forces
$d_y(x)$	Crack opening profile	Crack profile parameters
$d_{y,A} - d_{y,B}$	Difference between vertical displacements of points A and B (Fig. 2)	
U	Crack closure level	Closure parameters
σ_{op}/σ_{max}	Normalised opening stress	

Additionally, different parameters have been used to quantify crack closure, as indicated in Table 3. A widely used parameter is U, which defines the fraction of the load cycle for which the crack remains open, and is given by

$$U = \frac{P_{max} - P_{op}}{P_{max} - P_{min}}, \tag{1}$$

where P_{max} and P_{min} are the maximum and minimum loads in the load cycles and P_{op} is the opening load. This parameter ranges from 0 (crack always closed) to 1 (no closure). An alternative parameter also widely used is $(\sigma_{op}/\sigma_{max})$, ranging from $R = \sigma_{min}/\sigma_{max}$ (no closure) to 1. Distinct values are usually obtained for crack opening and crack closure.

Additional parameters have also been proposed to characterise the plastic wake and the near crack tip stress and strain fields, and have been used for a deeper understanding of crack tip phenomena and PICC. Antunes et al. [53] found that the crack profile, $d_y = d_y(x)$, is a main parameter influencing crack closure level. Rodrigues and Antunes [54] found that plastic deformation along the crack front stabilizes after a period that coincides with opening load stabilization, independently of the hardening model in use to describe the plastic behaviour of the material. Therefore the variation of equivalent plastic deformation along crack front $(d\bar{\varepsilon}^p_B/dx)$ can be used to identify the stabilization of the crack closure level.

2.2.4. Material model

Numerical simulation of the plastic behaviour of metals requires mechanical models that correctly describe the hardening behaviour of these materials [55]. In the specific situation of the numerical simulation of crack growth under cyclic loading, which involves cyclic plasticity phenomena inside the crack tip area, isotropic and kinematic hardening must be considered when modelling the plastic behaviour of the materials. This can be achieved by using mixed hardening constitutive models that enable the effects both of isotropic and kinematic hardening on plasticity to be captured. Unfortunately, although it is assumed that PICC is induced by crack tip cyclic plastic behaviour, most of the published studies on the numerical simulation of crack closure neglect actual metal hardening behaviour and model the stress–strain response of these materials as elastic-perfectly plastic [28,56] or bi-linear [21,32,42]. Several numerical studies employed material constitutive relationships that even ignore kinematic hardening [23,24,57] or simply consider pure isotropic or pure kinematic hardening material models [20,58]. Numerical simulation studies considering mixed hardening behaviour are still rare. Recently, Jiang et al. [35] published a comparative study considering three different mixed hardening models: the purely kinematic Prager–Ziegler hardening rule with an elastic–perfectly plastic (EPP) stress–strain relationship, the purely kinematic Prager–Ziegler hardening rule with a bilinear (BL) stress–strain relationship and a kinematic hardening model developed by the authors. In this study, they found a strong dependence of stabilized crack closure values on the mechanical model in use. These authors also discussed the inability

of the purely kinematic Prager–Ziegler hardening models, with an EPP stress–strain relationship, or a BL stress–strain relationship, to deal with strain ratcheting and stress relaxation under any loading conditions.

3. Numerical simulation of crack closure using a MT specimen

3.1. The numerical program

The numerical simulations were performed using a three-dimensional elasto-plastic finite element program (DD3IMP) that follows a fully implicit time integration scheme [59–61]. The use of an implicit algorithm makes the numerical code very robust.

The mechanical model and the numerical methods used in this finite element code, specially developed for the numerical simulation of metal forming processes, take into account the large elastic–plastic strains and rotations that are associated with large deformation processes. The quality of the solutions, provided by this numerical program, strongly relies on the models used to describe the strong non-linear material behaviour, which include several isotropic and anisotropic constitutive models (seven isotropic/kinematic hardening laws and eight yield criteria) [62,63]. In order to realistically define the geometry of the deformable body the numerical code makes use of three-dimensional solid isoparametric finite elements. Since the isoparametric elements have a deficient behaviour when used to solve elasto-plastic problems a selective reduced integration method [62,64] is adopted in this numerical simulation program in order to avoid the locking effect.

3.2. Finite element discretization of the cracked body

In this study a center cracked specimen (MT) subjected to plane stress mode *I* loading (Fig. 1a) was investigated (other authors have studied this geometry [21,25,28,35,45,46,65]). The geometry and size of the MT specimen, with initial crack size $a_o = 5.78$ mm, were chosen with reference to previous experimental work [3]. A relatively thin 0.2 mm section was considered in the numerical analysis, in order to simulate plane stress conditions. Due to symmetry conditions, only 1/8 of the sample was simulated, corresponding to the shadow portion in Fig. 1a. The 3D finite element mesh was obtained by generating one layer of eight-node isoparametric brick elements from a 2D mesh (Fig. 2). The size considered for the crack tip elements was $L_1 = 16$ μm.

All the simulations were performed assuming constant amplitude cyclic loading. The boundary conditions used in this investigation enforce frictionless contact conditions over a symmetry plane placed behind the growing crack front. Crack propagation was simulated by applying the commonly used one-node-per-two cycles debonding at minimum load. The increment at minimum load was adopted to overcome convergence difficulties. Each crack increment (Δa) corresponded to one finite element, i.e., $\Delta a = 16$ μm (see Fig. 3). In each cycle, the crack propagates uniformly over the thickness, by releasing both current crack front nodes. The opening load, P_{op}, necessary for the determination of the closure level is calculated by evaluating the contact status with the symmetry plane of the first node behind the current crack tip (reference node in Fig. 3). However, in Section 4.5 different concepts of crack closure have been considered and compared.

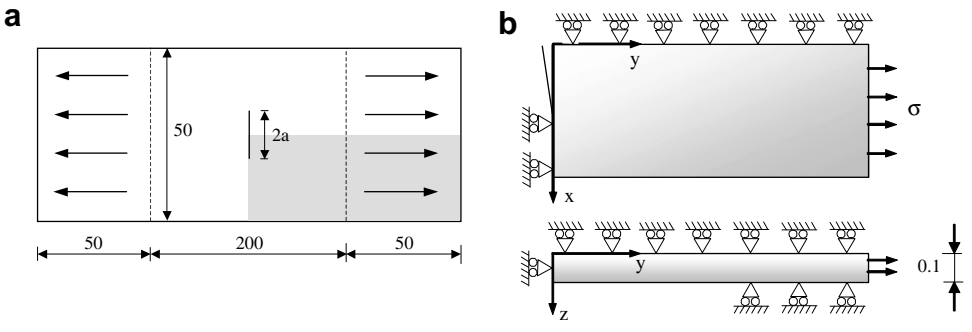

Fig. 1. (a) Middle-tension specimen M(T); (b) physical model.

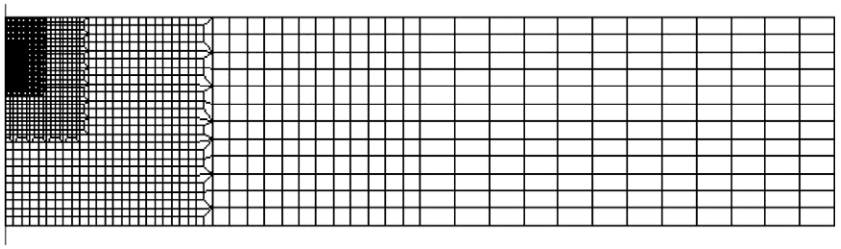

Fig. 2. Finite element mesh.

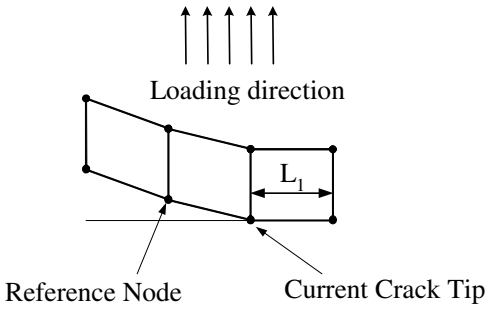

Fig. 3. Near crack tip elements.

3.3. Material modelling

The elasto-plastic behaviour of the material was modelled as corresponding to the AA6016-T4 aluminium alloy. Several monotonic and Bauschinger mechanical tests have been performed in order to study the hardening behaviour of this material. From the experimental data and curve fitting results, for different constitutive models, it was determined that the mechanical behaviour of this alloy is best represented using a isotropic hardening model described by a Voce type equation

$$Y = Y_0 + R_{\text{sat}}(1 - \mathrm{e}^{-n_{\text{v}}\bar{\varepsilon}^{\text{p}}}) \tag{2}$$

combined with a kinematic hardening model described by a saturation law [66]

$$\dot{X} = C_{\text{X}}\left[\frac{X_{\text{sat}}(\boldsymbol{\sigma}' - \mathbf{X})}{\bar{\sigma}} - \mathbf{X}\right]\dot{\bar{\varepsilon}}^{\text{p}}, \quad \text{with } \mathbf{X}(0) = 0. \tag{3}$$

In previous equations Y is the equivalent flow stress, $\bar{\varepsilon}^{\text{p}}$ is the equivalent plastic strain, Y_0 is the initial yield stress, R_{sat} is the saturation stress, n_{v}, C_{x} and X_{sat} are material constants, σ' is the deviatoric stress tensor, $\boldsymbol{X}$ is the back stress tensor, $\dot{\bar{\varepsilon}}^{\text{p}}$ the equivalent plastic strain rate and $\bar{\sigma}$ is the equivalent stress given by $\bar{\sigma}^2 = (\boldsymbol{\sigma}' - \mathbf{X}) : \mathbf{M} : (\boldsymbol{\sigma}' - \mathbf{X})$ where $\mathbf{M}$ is a fourth-order symmetric tensor which is function of the anisotropic parameters of the Hill'48 yield criterion: F, G, H, L, N and N. The material constants determined for the material in study are: $Y_0 = 124$ MPa, $R_{\text{sat}} = 291$ MPa, $n_{\text{v}} = 9.5$, $C_x = 146.5$, $X_{\text{sat}} = 34.90$ MPa, $F = 0.5998$, $G = 0.5862$, $H = 0.4138$ and $L = M = N = 1.2654$.

4. Presentation and analysis of results

4.1. Parameters of the numerical algorithm

The finite element program used in this study makes use of a Newton–Raphson method to solve the non-linear problem associated with the plastic deformation processes. The convergence of this numerical method depends mainly on parameters like the numerical variables, mechanical behaviour laws, the friction coefficient,

the discretization of the deformable body and the loading conditions. The optimum values for most of the numerical parameters of the DD3IMP implicit algorithm have been well established in previous investigations involving the numerical simulation of sheet metal forming processes [59,61], and are suitable for use in the study of the plastic deformation process occurring at the crack front. The only numerical parameter optimised in this work was a user defined constant (Toleq) that controls the global convergence of the Newton–Raphson algorithm and determines the precision of the numerical results. Fig. 4 presents the influence of Toleq on crack closure numerical results, expressed by U. The parameter optimization task was performed by determining the crack closure level (U) for a set of loading conditions characterised by increasing values of R (mean stress) and constant ΔK. The results indicate that the increase in R, fixing ΔK, produces an increase in U, which was expected. However, the increase in K_{max}, associated with the increase in R, increases plastic deformation at the crack tip. Therefore, more precision is required in order to correctly capture the stress–strain gradients at the crack tip, which means that lower values of Toleq have to be used, as Fig. 4 shows. These results reinforce the importance of careful control of the numerical algorithm to ensure the quality of numerical results. In any case, the results from crack tip elements, and particularly, at the crack tip node, are always affected by errors resulting from the singular character associated with sharp cracks.

4.2. Radial size of crack front elements, L_1

The radial size of the crack tip elements (L_1) is a main parameter of the numerical model and must be carefully defined. Its maximum value may be established based on the size of the reversed plastic zone and the measurement of this size is a central issue. Solancki et al. [28] analysed the equivalent Von Mises stress (σ_{VM}) at maximum and minimum load and considered the criterion $0.95 \leqslant \sigma_{VM}/\sigma_{ys} \leqslant 1$ to define the limits of the reversed plastic zone. Alternatively, the reversed zone can be defined by comparing the equivalent plastic deformation, along the crack front, at maximum and minimum loads. The increase in plastic deformation with the decrease in load, down to its minimum value, indicates the occurrence of reversed plasticity. Fig. 5 shows the application of these two concepts, and both indicate that approximately 3–4 elements are within the reversed plastic zone (shadow region).

The size of the reversed zone can also be determined from the analysis of stress–strain curves of near crack tip points. Fig. 6a presents a normalized stress–strain curve ($\sigma_{yy} - \varepsilon_{yy}$) registered as the crack propagates ($\Delta a = 15 \times 16 = 240$ μm) for a Gauss point (GP) positioned as illustrated in Fig. 6b. Notice that two load cycles were applied between crack extensions. At the end of the first cycle (crack tip in position 1) the GP suffers some plastic deformation, which indicates that it is within the forward plastic zone, but does not

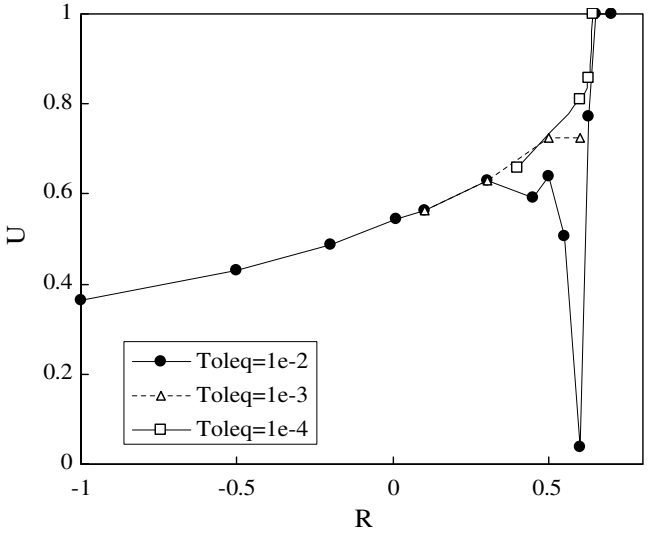

Fig. 4. Closure level (U) versus stress ratio (R) after 15 propagation cycles ($a = 6.004$ mm; $\Delta K = 5.2$ MPa m$^{1/2}$; $L_1 = 16$ μm).

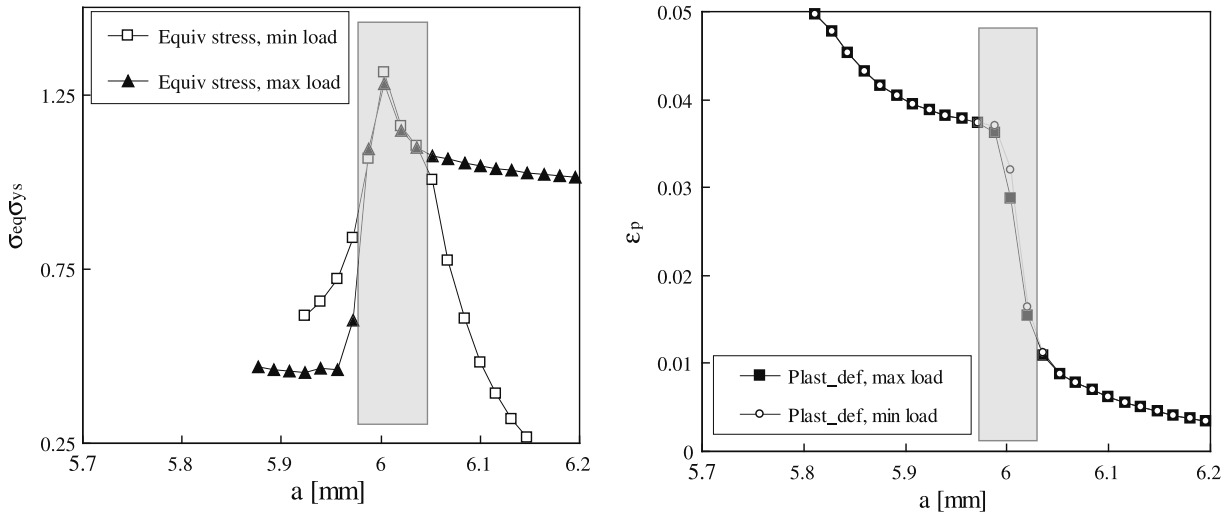

Fig. 5. Identification of reversed plastic zone ($\sigma_{max} = 40$ MPa, $\sigma_{min} = 4$ MPa, $a_0/W = 0.23$, $L_1 = 16$ μm, $\Delta a = 15 \times 16$ μm $= 240$ μm, two cycles per increment).

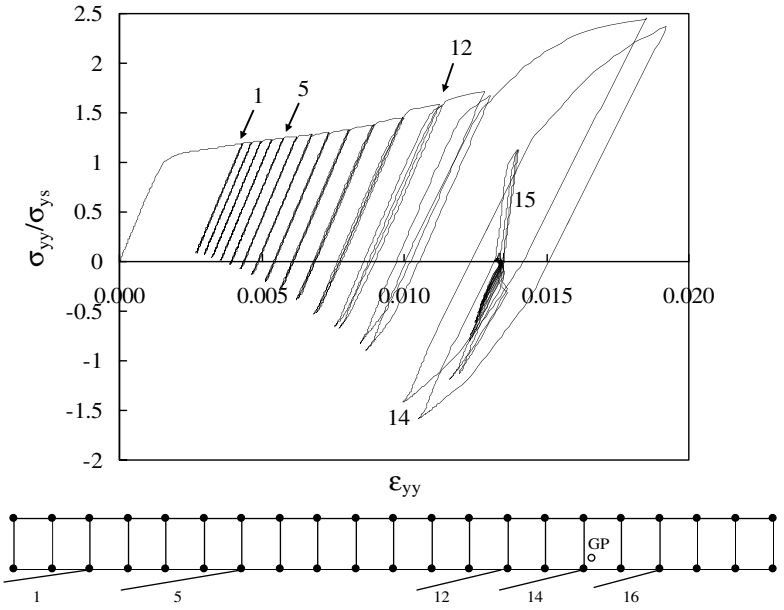

Fig. 6. (a) Stress–strain curve for one Gauss point; (b) location of the Gauss point relatively to the crack tip ($\sigma_{max} = 40$ MPa, $\sigma_{min} = 4$ MPa, $a_0/W = 0.23$, $L_1 = 16$ μm, $\Delta a = 20 \times 16$ μm $= 320$ μm, two cycles per increment).

experience reversed plasticity. After five crack increments (crack tip in position 5), compressive stresses arise at the GP position. These compressive stresses increase with the approximation of the crack tip and start producing reversed plasticity after 12 load cycles (crack tip in position 12). The reversed plastic zone increases up to 14 crack increments, therefore three elements are within this zone, which is in accordance with the analysis in Fig. 5. After 15 crack increments, crack propagation extends ahead of the GP position, the level of stress applied to the GP becomes relatively low and the increment of plastic deformation quite reduced. In other words, the plastic wedge develops up to position 14. Points with other vertical positions (y coordinate in Fig. 1b) were observed to have similar behaviour, however the level of monotonic and reversed plastic deformation vary significantly.

The analysis of the stress–strain curve is probably the best procedure for quantifying the size of the reversed plastic zone and, thus, for defining L_1. If L_1 is too high, even the GP closest to the crack tip does not suffer reversed plastic deformation. For $L_1 = 16$ μm, a significant portion of the cyclic plastic deformation occurs within the three elements ahead of crack tip. However, inside this zone the points are submitted to only six load cycles, which is far from reality. The decrease in L_1 and the increase in the number of load cycles, between crack increments, increase the total number of load cycles, as discussed in Section 4.4.

4.3. Crack extension for stabilization, Δa_{stb}

Under constant amplitude loading the crack tip opening load will typically increase monotonically with increasing crack growth until a stabilized value is reached. So, it is important to define the minimum crack extension needed to stabilize the opening level, that is equal to the sum of the partial crack increments, i.e., $\Delta a_{\mathrm{stb}} = \sum(\Delta a)_i$, with i varying from 1 to the number of increments necessary for stabilisation. Parks et al. [38] suggested that to achieve closure stabilised values, the crack must propagate ahead of the monotonic plastic zone resulting from the first load cycle (r_{p}). Wu and Ellyin [48] found that under plane stress conditions the opening level reaches a stable value when the crack tip propagates over half of the initial plastic zone. Antunes et al. [43] found that, for a plane stress state, the crack must propagate ahead of Rice's monotonic plastic zone of first load cycle. Solancki et al. [28] and Jiang et al. [35] indicated that the steady state was reached after growing the crack approximately twice and four times the initial forward plastic zone, respectively. Considering these different results, it is recommended that a convergence study should always be developed.

Fig. 7 shows stabilization results obtained in this study for $R = 0.1$ and 0.5. The crack tip finite element mesh is schematized at the bottom of the graph. The opening level results are expressed by ($\sigma_{\mathrm{open}}/\sigma_{\mathrm{max}}$) being σ_{open} determined as described in [45]. The load versus opening displacement curve for the node behind crack tip exhibits linear behaviour, therefore the exact opening load can be obtained by extrapolation of the two load values following opening.

This procedure eliminates the small error associated with the evaluation of the opening load at the end of load increments with finite size. It can be seen that the closure level increases, with initial crack propagation, until a stable value is reached, which is also demonstrated by the $\mathrm{d}(\sigma_{\mathrm{open}}/\sigma_{\mathrm{max}})/\mathrm{d}x$ curve. These results indicate the decreasing influence of the first plastic wedge as the crack propagates. Immediately behind the crack tip, the plastic wake has a major influence on closure level, which decreases rapidly with crack propagation until it

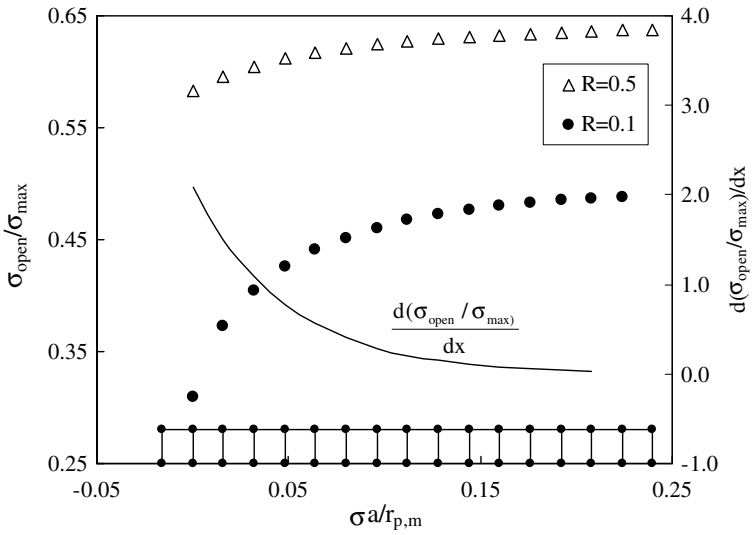

Fig. 7. Crack closure stabilization: numerical results and extrapolation models (Toleq = 1e − 4, $L_1 = 16$ μm, two load cycles, $\Delta a = 15 \times 16$ μm = 240 μm, $\sigma_{\mathrm{max}} = 40$ MPa, $R = 0.1$, $r_{\mathrm{p,m}} = 0.618$ mm).

disappears. This decreasing influence can be explained by a lever effect: the rotation imposed by a remote plastic wedge produces a small vertical movement near the crack tip. This lever effect explains the lower stabilization period required for plane strain conditions [23,36]. In fact, crack opening is larger at interior positions of the crack front, therefore the effect of the remote plastic wake is lower. In general, all modifications of physical parameters that promote an increase in crack opening displacement, like the increase in mean stress or change of specimen geometry, will reduce the extent of the stabilization process. This effect of mean stress on stabilization process is obvious from the results presented in Fig. 7 for $R = 0.1$ and 0.5.

In situations with very small element sizes and where long propagation is required for stabilization, it is interesting to perform extrapolation of crack closure values in order to perform a limited number of crack propagations and save numerical simulation time. González-Herrera and Zapatero [36] and Jiang et al. [35], respectively, proposed the following extrapolation models:

$$\frac{\sigma_{open}}{\sigma_{max}} = k - \frac{1}{\left(\frac{\Delta a}{r_p} + c\right)^b}, \tag{4}$$

$$\frac{\sigma_{open}}{\sigma_{max}} = C_0 + C_1 \cdot e^{C_2 \cdot \Delta a}. \tag{5}$$

Both models have three fitting constants, k and C_0 being the horizontal asymptotes. Fig. 8 presents the fitting of these models to previous numerical results. The extrapolated values were found to be reasonable, but not excellent, therefore a new model is proposed here, which is a modified version of Eq. (5):

$$\frac{\sigma_{max}}{\sigma_{open}} = C_0 + C_1 \cdot e^{C_2 \cdot \Delta a^{C_3}} \tag{6}$$

This equation, which is a Voce type equation similar to that used to model the isotropic hardening behaviour of the material (Eq. (2)), has four constants. The extrapolation results obtained with this model are compared, in Fig. 8, with those obtained with previous models and show that the best fit is obtained with Eq. (6). Fig. 8 also presents some extrapolated values calculated with the proposed model, but considering different and increasing numbers of crack increments (3, 4, 5,...). It is possible to observe that as the crack propagates, the extrapolated values stabilize, achieving this stabilized value after about eight crack extensions (128 μm).

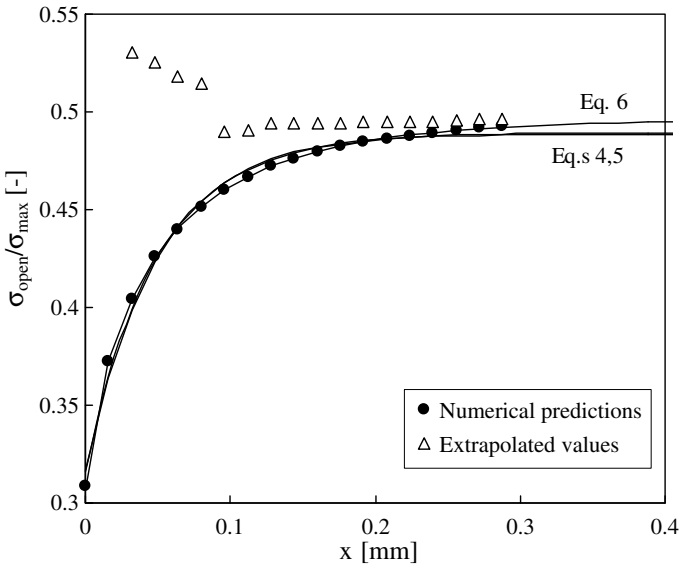

Fig. 8. Extrapolation of the extrapolated values ($B = 0.2$ mm, Toleq = 1e − 4, $L_1 = 16$ μm, two load cycles, $\Delta a_{max} = 18 \times 16$ μm = 288 μm, $R = 0.1$, $\sigma_{max} = 40$ MPa).

4.4. Effect of the number of load cycles, NLC

The number of load cycles applied to the near crack tip points depends on the size of the individual crack increments ($\Delta a_i = L_1$) and on the number of load cycles between crack propagations. The influence of NLC is greatly dependent on the elastic–plastic model assumed for the material, particularly, on the capacity of the model to simulate mean stress relaxation, strain ratcheting and cyclic hardening. Ideally, the FCGR in the numerical model should be similar to the experimental one. However, when using a mesh of 16 μm and a one-node-per-two cycles debonding scheme, an unrealistic fatigue crack growth of 8×10^{-6} m/cycle is simulated, which is significantly higher than real da/dN. Reducing the mesh size or increasing the number of load cycles between crack propagations, up to a realistic level, is not practical due to the huge numerical effort involved. The objective now is to understand the effect of increasing the number of load cycles, considering that realistic FCGR cannot be reached.

Fig. 9 presents the normalized σ_{yy} versus ε_{yy} curve obtained, for the same Gauss point illustrated in Fig. 6b, but using different test conditions, i.e., four load cycles between crack extensions. The comparison with Fig. 6a indicates that the application of more load cycles slightly increases the plastic strain at the GP. Strain ratcheting and mean stress relaxation are evident in Fig. 9 and stabilization would occur with the application of more load cycles between crack increments. Fig. 10 shows the influence of the number of load cycles between crack propagations on the crack opening level ($\sigma_{open}/\sigma_{max}$). A significant difference between the results obtained with 1 cycle and 2 cycles can be observed, while the subsequent number of load cycles has a limited effect. This difference can be explained by the crack opening profile behaviour. The second load cycle slightly deforms the fracture surface, reducing the closure level. Therefore at least two load cycles between each crack increment must be applied [20,30,38].

The effect of using more than two load cycles in crack closure behaviour is intimately related to the material model in use. For mixed hardening models stabilization of the opening level is observed, which can be explained by the stabilization of cyclic plastic deformation. The small difference between the results of Figs. 6a and 9 obtained for NLC of 2 and 4, respectively, agree with the small difference observed in Fig. 10.

It was also observed that the application of load cycles in a MT specimen, without crack extension, produces an interesting phenomenon in specific situations. Fig. 11 shows the variation of the near crack tip profile in a numerical simulation performed considering pure kinematic hardening behaviour. The crack was submitted to 15 propagations with 2 load cycles between each, and after that, 20 load cycles were applied without propagation. As can be concluded from the figure, the increasing number of load cycles affects the position of the node immediately behind the crack tip, moving it upward. Therefore, the first two loading cycles

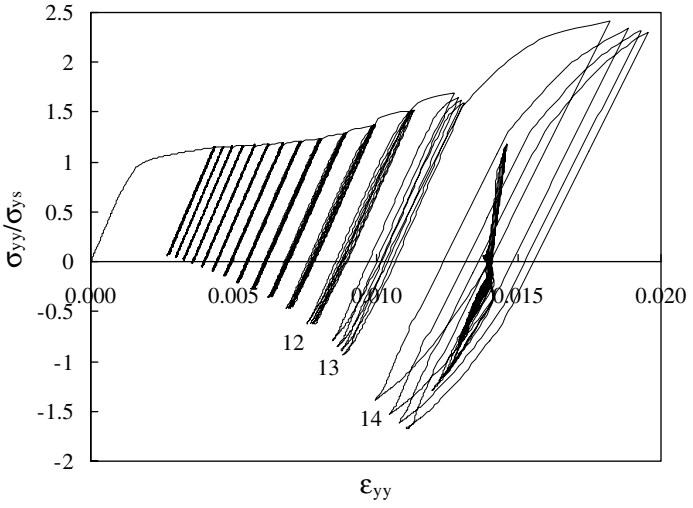

Fig. 9. Stress–strain curve for one Gauss point ($\sigma_{max} = 40$ MPa, $\sigma_{min} = 4$ MPa, $a_0/W = 0.23$, $L_1 = 16$ μm, $\Delta a = 20 \times 16$ μm $= 320$ μm, four cycles per increment).

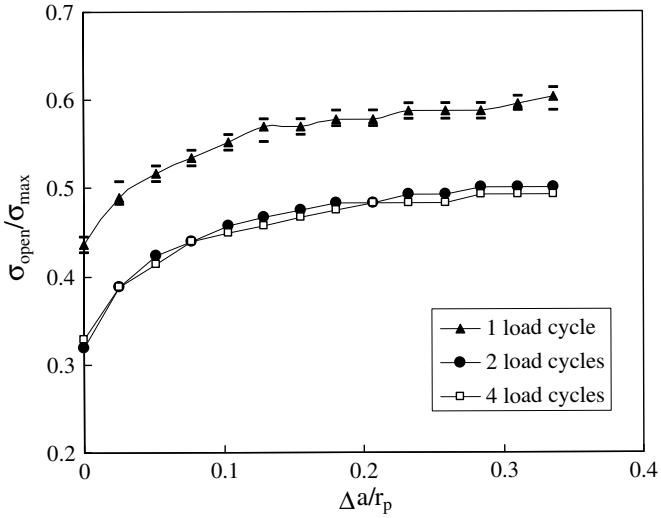

Fig. 10. Effect of the number of load cycles between propagations ($\sigma_{max} = 40$ MPa, $R = 0.1$, $L_1 = 16$ μm, $\Delta a = 15 \times 16$ μm $= 240$ μm and $r_{p,m} = 0.618$ mm).

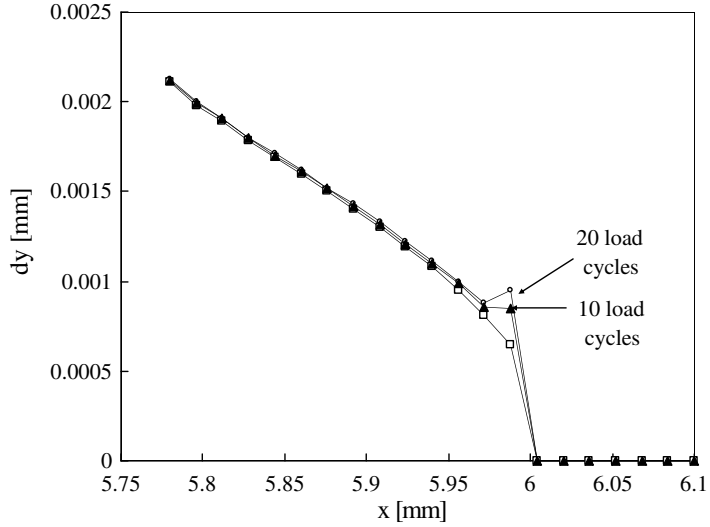

Fig. 11. Crack profiles for different numbers of load cycles without crack propagation for pure kinematic hardening ($\Delta a = 15 \times 16$ μm $=$ 240 μm, $L_1 = 16$ μm).

produce plastic deformation, and consequently, crack closure. Subsequent unloading and loading cycles take material from behind the crack tip, reducing closure. A similar phenomenon was observed for elastic – perfect plastic behaviour. This geometrical change explains the reduction of closure level with an increasing number of load cycles/increments for pure kinematic hardening and perfect plastic material behaviour (results not presented). This effect was studied using different meshes and it was concluded that it is mesh-size dependent, being more important for a mesh with $L_1 = 8$ μm. Whatever the mesh size is, only the node immediately behind the crack tip node is moved. No significant effect of an increasing number of load cycles on the crack profile of non-propagating cracks was observed when using mixed hardening models, which indicates that the phenomenon depends on material behaviour modelling. The same phenomenon has also been reported by Antunes et al. [43] and Jiang et al. [35] for pure kinematic hardening models in 2D plane stress analysis. Toribio and Kharin [67] developed a high-resolution finite-element simulation of a plane strain tensile crack

with a finite radius. Perfect plastic behaviour was assumed and deformed shapes revealed the mechanism of material transfer from the crack front onto the lateral faces of the crack.

4.5. Closure definition

Fig. 12 presents values obtained for the opening level, $\sigma_{open}/\sigma_{max}$, based on the last contact of different nodes behind the crack tip. A major conclusion that can be drawn from this graph is the great variation in closure results (from 0.3 to 0.49) according to the node selected to evaluate contact status. As expected, remote nodes open first and a linear variation in closure is observed between the results of the 6th and 9th nodes. This variation becomes much more significant when choosing nodes closest to the crack tip to evaluate contact status, i.e., it is more difficult to open these nodes. This effect is explained by the occurrence of plastic deformation at the crack tip at the same time that the nodes closest to the crack tip are opening.

The value of $\sigma_{open}/\sigma_{max}$ obtained from the stress inversion definition is also presented in Fig. 12. This value is higher than that obtained from the first node behind the current crack tip. In fact, the contact status of this node does not indicate that the crack is fully open, i.e., that the crack is open between this node and the current crack tip node. Reducing L_1 is expected to reduce the difference between both definitions of crack closure. A strong agreement can be observed between the result from the stress inversion definition and that obtained from the extrapolation $L_1 \to 0$ of the opening values from the nodes behind crack tip, as could be expected.

The opening value obtained from remote displacement values, which is equivalent to that found by experimental measurements procedure, is also presented in Fig. 12. The vertical displacements of a node at $x = 0$, $y \approx 2$ mm were registered and closure was determined using the maximization of the correlation coefficient [68]. The resulting opening value agrees with the opening results from node 5. Antunes et al. [43] found agreement with node 1 from crack tip in a 2D analysis.

4.6. Effect of stress ratio, R

Fig. 13a presents predictions of crack opening level U obtained by fixing the stress range and increasing the minimum and maximum stresses, as is schematised in Fig. 13b. Each type of cycle in Fig. 13b corresponds to one numerical prediction (•) in Fig. 13a. The ratio σ_{max}/σ_{ys} varies from 0.14 to 0.78 when the stress ratio varies from −1 to 0.64. The first node behind the crack tip was used to quantify the crack opening level. From this

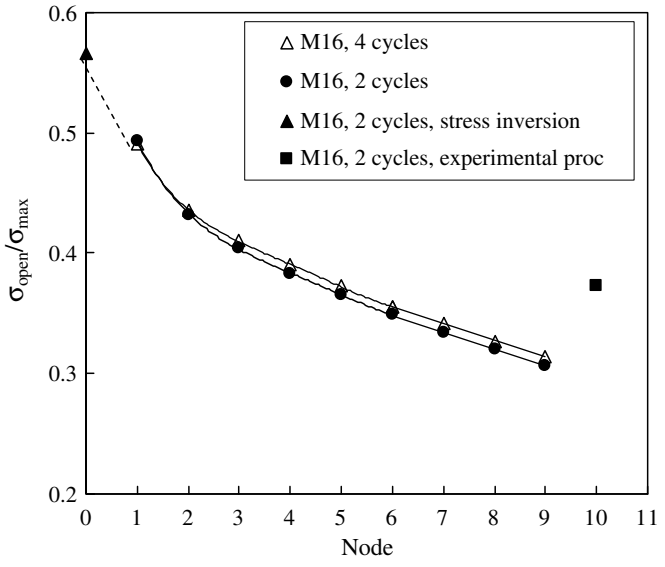

Fig. 12. Influence of crack opening definition (Toleq = 1e − 4, $\sigma_{max} = 40$ MPa, $\sigma_{min} = 4$ MPa, $a_0/W = 0.23$, $L1 = 16$ μm, $\Delta a = 15 \times 16$ μm = 240 μm, two cycles per increment).

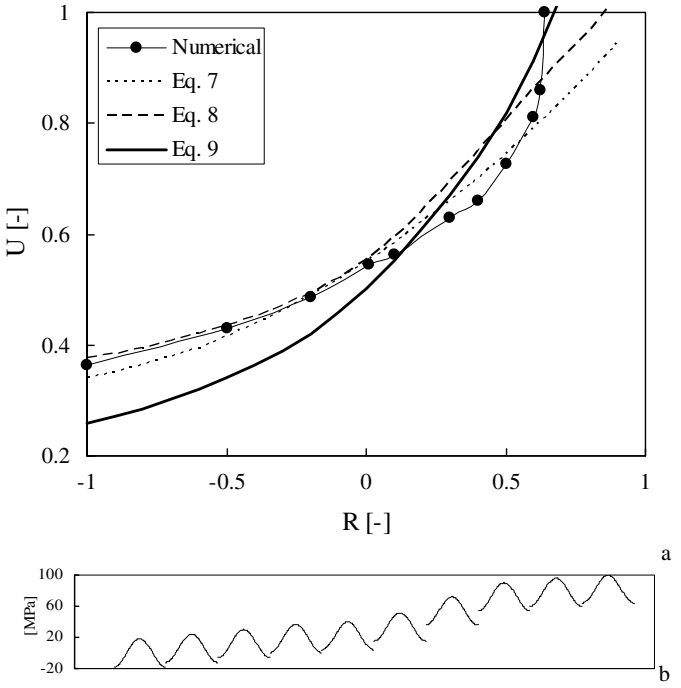

Fig. 13. Effect of R fixing ΔK ($a/W = 0.24$, $\Delta\sigma = 36$ MPa, $L_1 = 16$ μm, $\Delta a = 15 \times 16$ μm $= 240$ μm).

diagram it is possible to conclude that the increase in the mean stress produces a clear increase in U. For $R > 0.64$ no closure is observed numerically, i.e., $U = 1$.

Schijve [69], based on the work of Newman [47], proposed the equation

$$\frac{\sigma_{op}}{\sigma_{max}} = 0.45 + 0.22R + 0.21R^2 + 0.12R^3 \tag{7}$$

to describe the variation of the opening level ($\sigma_{open}/\sigma_{max}$) with R. In the same year, de Koning [70] proposed the following model for the 7075-T6 aluminium alloy:

$$\frac{\sigma_{op}}{\sigma_{max}} = \begin{cases} \left(1 - 0.25(1-R)^3 \frac{\sigma_{max}}{\sigma_{ys}}\right)(0.45 + 0.2R - 0.15R^2 + 0.9R^3 - 0.4R^4) & R > 0 \\ \left(1 - 0.25(1-R)^3 \frac{\sigma_{max}}{\sigma_{ys}}\right)(0.45 + 0.2R) & R \leqslant 0. \end{cases} \tag{8}$$

Newman [71] calculated the crack opening stress for CCT specimens subjected to uniaxial constant amplitude loading and proposed the following equations

$$\begin{aligned} \frac{\sigma_{op}}{\sigma_{max}} &= A_0 + A_1 \cdot R + A_2R^2 + A_3R^3 \qquad R \geqslant 0 \\ \frac{\sigma_{op}}{\sigma_{max}} &= A_0 + A_1 \cdot R \qquad -1 \leqslant R < 0 \end{aligned} \tag{9}$$

where A_{is} are empirical factors given by

$$\begin{aligned} A_0 &= (0.825 - 0.34\alpha + 0.05\alpha^2)\left[\cos\left(\frac{\pi}{2}\frac{\sigma_{max}}{\sigma_0}\right)\right]^{1/\alpha} \\ A_1 &= (0.415 - 0.071\alpha)\frac{\sigma_{max}}{\sigma_0} \\ A_2 &= 1 - A_0 - A_1 - A_3 \\ A_3 &= 2A_0 + A_1 - 1. \end{aligned} \tag{10}$$

The equation is a function of stress ratio R, stress level, σ_{max} and three-dimensional constraint factor α. Flow stress σ_0 is taken to be the average between the uniaxial yield stress and uniaxial ultimate tensile strength of the material. Generally plane stress or plane strain conditions are simulated with $\alpha = 1$ or 3, respectively. A value $\alpha = 1$ was assumed considering that a plane stress state is being studied.

The predictions of $\sigma_{max}/\sigma_{open}$ obtained according these three models were used to obtain U (Eq. (1)) and the results are plotted in Fig. 13a. Despite the discrepancies in loading conditions, materials and closure definition, a strong agreement exists between the empirical models and the numerical predictions. A good agreement can be found between the predictions based on Eqs. (7) and (8) and the numerical simulation results up to $R = 0$.

5. Conclusions

This paper is a numerical study of the main parameters affecting plasticity induced crack closure. The main aspects and conclusions of this study are:

- a numerical model of PICC was developed and implemented using the proprietary DD3IMP code. The model maintains the main limitations of the literature models, namely discrete crack propagations, a relatively high fatigue crack growth, sharp cracks and crack propagation at a well defined load. However, contrary to most literature studies, a mixed hardening model was assumed, consisting of a Voce type law combined with kinematic hardening described by a saturation law;
- the physical parameters and the numerical parameters were systematically identified. The dependent parameters used in the literature to quantify crack closure level and crack tip phenomena were also discussed;
- the numerical parameters were divided into two main groups: those affecting the results of predictions (parameters of numerical algorithm, radial size of crack tip elements and minimum crack propagation for stabilization) and those responsible for the intrinsic uncertainty of the numerical modelling of PICC;
- a study was developed to optimize the numerical predictions. The parameter named Toleq, that controls the global convergence of the Newton–Raphson algorithm, was optimized. The minimum radial size of crack tip elements, L_1, necessary to model adequately reversed plasticity, was studied. The analysis of the stress–strain curve for a Gauss point close to the crack tip was found to be sufficient to ensure that reversed plastic deformation is being adequately modelled and to define an upper limit for L_1. The convergence of closure values with crack propagation was studied, and extrapolation models compared. Excellent results were obtained with the Voce model, usually used to model material behaviour. The study of these three parameters is fundamental to ensure feasible results, and must be done for each set of physical parameters;
- despite all efforts to obtain accurate results, closure predictions will always be affected by an intrinsic uncertainty. Main parameters affecting this intrinsic uncertainty are the number of load cycles applied to near crack tip points (NLC) and the definition of closure. The NLC depends on L_1 and on the number of load cycles between crack propagations. A convergence of the opening values was found with the increase in NLC, explained by the stabilization of cyclic curves. The definition of closure is probably the main source of uncertainty;
- the numerical models are ideal for studying the influence of physical parameters. For that, the parameters affecting the accuracy must be optimized, and the parameters of uncertainty fixed;
- the effect of stress ratio (fixing ΔK) was studied. A reasonable agreement was found with empirical models found in literature.

Acknowledgement

The authors acknowledge the financial support provided by Fundação para a Ciência e Tecnologia, Portugal (Project POCTI/EME 47022/2002) and UE/FEDER.

References

[1] Elber W. The significance of fatigue crack closure under cyclic tension. ASTM STP 1971;486:230–42.
[2] Blom AF, Holm DK. An experimental and numerical study of crack closure. Engng Fract Mech 1984;22:997–1011.

[3] Borrego LFP. Fatigue crack growth under variable amplitude loading in AlMgSi aluminium alloys. PhD thesis. University of Coimbra: Portugal; 2001.
[4] Christensen RH. Fatigue crack growth affected by metal fragments wedged between opening–closing crack surfaces. Appl Mater Res 1963;2(4):207–10.
[5] Elber W. Fatigue crack closure under cyclic tension. Engng Fract Mech 1970;2:37–45.
[6] James MN. Some unresolved issues with fatigue crack closure – measurement, mechanism and interpretation problems. In: Karihaloo BL, Mai Y-W, Ripley MI, Ritchie RO, editors. Ninth international conference on fracture. Pergamon Press; 1997. p. 2403–14.
[7] Ritchie RO, Zurres S, Moss CM. Near-threshold fatigue crack growth in 2(1/4)Cr-1 Mo pressure vessel steel in air and hydrogen. J Engng Mater Technol 1980;102:293–9.
[8] Suresh S, Ritchie RO. On the influence of fatigue underloads on cyclic crack growth at low stress intensities. Mater Sci Eng 1981;51:61–9.
[9] Suresh S, Ritchie RO. A geometric model for fatigue crack closure induced by fracture surface morphology. Metallur Trans 1982;13A:1627–31.
[10] Tzou JL, Suresh S, Ritchie RO. Fatigue crack propagation in oil environments, I-crack growth in silicone and paraffin oils. Acta Metallur 1985;33:105–16.
[11] Pineau AG, Pelloux RM. Influence of strain induced martensitic transformations on fatigue crack growth rates in stainless steels. Metallur Trans 1974;5:1103–12.
[12] Takeshio O, Koboyshi H. Near-threshold fatigue crack growth and crack closure in a nodular cast iron. Fatigue Fract Engng Mater Struct 1987;10:273–80.
[13] Louat N, Sadananda K, Duesbery M, Vasudevan AK. A theoretical evaluation of crack closure. Metallur Trans 1993;24A:2225–32.
[14] Vasudeven AK, Sadananda K, Louat N. A review of crack closure, fatigue crack threshold and related phenomena. Mater Sci Engng 1994;A188:1–22.
[15] Sadananda K, Vasudevan AK, Holtz RL, Lee EU. Analysis of overloads effects and related phenomena. Int J Fatigue 1999;21:S233–46.
[16] Kumar R. Review on crack closure for constant amplitude loading in fatigue. Engng Fract Mech 1992;42:389–400.
[17] Wang GS. The plasticity aspect of fatigue crack growth. Engng Fract Mech 1993;46(6):909–30.
[18] Laird C, Smith GL. Initial stages of damage in high stress fatigue in some pure metals. Phil Mag 1963;95(8):1945–63.
[19] Laird C. The influence of metallurgical structure on the mechanisms of fatigue crack propagation. ASTM STP 1967;415:247–309.
[20] Pommier S, Bompard Ph. Bauschinger effect of alloys and plasticity-induced crack closure: a finite element analysis. Fatigue Fract Engng Mater Struct 2000;23:129–39.
[21] Roychowdhury S, Dodds Jr RH. A numerical investigation of 3D small-scale yielding fatigue crack growth. Engng Fract Mech 2003;70:2363–83.
[22] Wei L-W, James MN. A study of fatigue crack closure in polycarbonate CT specimens. Engng Fract Mech 2000;66:223–42.
[23] Skinner JD, Daniewicz SR. Simulation of plasticity-induced fatigue closure in part-through cracked geometries using finite element analysis. Engng Fract Mech 2002;69:1–11.
[24] Zhang JZ, Bowen P. On the finite element simulation of three-dimensional semi-circular fatigue crack growth and closure. Engng Fract Mech 1998;60(3):341–60.
[25] Chermani RG, Shivakumar KN, Newman Jr JC, Blom AF. Three-dimensional aspects of plasticity-induced fatigue crack closure. Engng Fract Mech 1989;34(2):393–401.
[26] Ellyin F, Wu J. A numerical investigation on the effect of an overload on fatigue crack opening and closure behaviour. Fatigue Fract Engng Mater Struct 1999;22:835–47.
[27] Cordero A, García-Manrique J, Moreno B, Zapatero J, González-Herrera A. Estudio numérico del efecto en el cierre en fatiga de la longitud de grieta. Anales de Mecánica de la Fractura 2003;20:53–8.
[28] Solanki K, Daniewicz SR, Newman Jr JC. Finite element modelling of plasticity-induced crack closure with emphasis on geometry and mesh refinement effects. Engng Fract Mech 2003;70:1475–89.
[29] Simandjuntak S, Alizadeh H, Smith DJ, Pavier MJ. Three dimensional finite element prediction of crack closure and fatigue crack growth rate for a corner crack. Int J Fatigue 2006;25:335–45.
[30] Pommier S. A study of the relationship between variable level fatigue crack growth and the cyclic constitutive behaviour of steel. Int J Fatigue 2001:S111–8.
[31] Pommier S, Freitas M. Effect on fatigue crack growth of interactions between overloads. Fatigue Fract Engng Mater Struct 2002;25:709–22.
[32] McClung RC, Sehitoglu H. On the finite element analysis of fatigue crack closure-2: numerical results. Engng Fract Mech 1989;33:253–72.
[33] Pommier S. Plain strain crack closure and cyclic hardening. Engng Fract Mech 2002;69:25–44.
[34] García-Manrique J, Cordero A, Pascual J, Zapatero J, González-Herrera A. Influencia de los modelos de plastificación en la simulación por elementos finitos del cierre en fatiga. Anales de Mecánica de la Fractura 2003;20:65–70.
[35] Jiang Y, Feng M, Ding F. A re-examination of plasticity-induced crack closure in fatigue crack propagation. Int J Plasticity 2005;21:1720–40.
[36] González-Herrera A, Zapatero J. Influence of minimum element size to determine crack closure stress by the finite element method. Engng Fract Mech 2005;72:337–55.
[37] Kim J-S, Kang JY, Song J-H. Elucidation of fatigue crack closure behaviour in surface crack by 3D finite element analysis. Int J Fatigue 2007;29:168–80.

[38] Parks S-J, Earmme Y-Y, Song J-H. Determination of the most appropriate mesh size for a 2D finite element analysis of fatigue crack closure behaviour. Fatigue Fract Engng Mater Struct 1997;20(4):533–45.
[39] Ogura K, Ohji K. FEM analysis of crack closure and delay effect in fatigue crack gowth under variable amplitude loading. Engng Fract Mech 1977;9:471–80.
[40] Ogura K, Ohji K, Honda K. Influence of mechanical factors on the fatigue crack closure. Advances in research on the strength and fracture of materials (fracture 1977). In: Proceedings of the fourth International Conference on Fracture Mechanics, vol. 2D. Waterloo, Canada; 1977. p. 1035–47.
[41] Palazotto AN, Mercer JG. A finite element comparison between short and long cracks within a plastic zone due to a notch. Engng Fract Mech 1990;35:967–86.
[42] McClung RC, Sehitoglu H. On the finite element analysis of fatigue crack closure-1: basic modelling issues. Engng Fract Mech 1989;33(2):237–52.
[43] Antunes FV, Borrego LFP, Costa JD, Ferreira JM. A numerical study of fatigue crack closure induced by plasticity. Fatigue Fract Engng Mater Struct 2004;27(9):825–36.
[44] Solanki K, Daniewicz SR, Newman Jr JC. A new methodology for computing crack opening values from finite element analysis. Engng Fract Mech 2004;71:1165–75.
[45] Alizadeh H, Hills DA, de Matos PFP, Nowell D, Pavier MJ, Paynter RJ, et al. A comparison of two and three-dimensional analyses of fatigue crack closure. Int J Fatigue 2007;29:223–31.
[46] Solanki K, Daniewicz SR, Newman Jr JC. Finite element analysis of plasticity-induced crack closure: an overview. Engng Fract Mech 2004;71:149–71.
[47] Newman Jr JC. A finite element analysis of fatigue crack closure. ASTM STP 1976;590:281–301.
[48] Wu J, Ellyin F. A study of fatigue crack closure by elastic–plastic finite element analysis for constant-amplitude loading. Int J Fract 1996;82:43–65.
[49] Sun W, Sehitoglu H. Residual stress fields during fatigue crack growth. Fatigue Fract Engng Mater Struct 1989;15:115–28.
[50] Sehitoglu H, Sun W. Modelling of plane strain fatigue crack closure. ASME J Eng Mat Technol 1991;113:31–40.
[51] Hellyin F, Wu J. A numerical investigation on the effect of an overload on fatigue crack opening and closure behaviour. Fatigue Fract Engng Mater Struct 1999;22:835–47.
[52] Shterenlikht A, Días-Garrido FA, Lopez-Crespo P, Withers PJ, Yates JR, Patterson EA. Mixed mode (K_II + K_II) stress intensity factor measurement by electronic speckle pattern interferometry and image correlation. Appl Mech Mater 2004;1–2: 107–12.
[53] Antunes FJV, Rodrigues DM, Ferreira JAM. Simulação numérica do fecho de fenda: Alguns aspectos associadosà discretização por elementos finitos. In: Mota Soares CA, et al., editors. Congresso de Métodos Computacionais em Engenharia. Associação Portuguesa de Mecânica Teórica, Aplicada e Computacional, Lisboa; 2004. p. 309.
[54] Rodrigues DM, Antunes FV. Numerical Simulation of plasticity induced crack closure in 6xxx aluminium alloys: effect of work hardening modelling. In Fourth international alloy conference (IAC 4), Kos, Greece; 2005.
[55] Bouvier S, Alves JL, Oliveira MC, Menezes LF. Modeling of anisotropic work-hardening behaviour of metallic materials subjected to strain-path changes. ComputMater Sci 2005;32(3–4):301–15.
[56] Fleck NA, Newman Jr JC. Analysis of crack closure under plain strain conditions. In: Newman Jr JC, Elber W, editors. Mechanics of fatigue crack closure. ASTM STP, vol. 982. Philadelphia: American Society for Testing and Materials; 1988. p. 319–41.
[57] Chermahini RG, Palmberg B, Blom AF. Fatigue crack growth and closure behaviour of semicircular and semielliptical surface flaws. Int J Fatigue 1993;15:259–63.
[58] Toyosada M, Gotoh K. The significance of plastic zone growth under cyclic loading and crack opening/closing model in fatigue crack propagation. Mater Sci Forum 2005;482:95–102.
[59] Menezes LF, Teodosiu C. Three-dimensional numerical simulation of the deep-drawing process using solid finite elements. J Mater Process Technol 2000;97:100–6.
[60] Alves L, Oliveira MC, Menezes LF. An advanced constitutive model in sheet metal forming simulation: the Teodosiu microstructural model and the Cazacu Barlat yield criterion. In: Ghosh S, Castro JM, Lee JK, editors. NUMIFORM, 2004. American Institute of Physics; 2004. p. 645–1650.
[61] Oliveira MC, Menezes LF. Automatic correction of the time step in implicit simulations of the stamping process. Finite Elem Anal Des 2004;40:1995–2010.
[62] Menezes LF, Thuiller S, Manach PY, Bouvier S. Influence of the work-hardening models on the numerical simulation of a reverse deep-drawing process. In: Khan AS, Lopez-Pamies O, editors. Plasticity'02. Neat Press; 2001. p. 331–3.
[63] Alves JL, Oliveira MC, Menezes LF. Influence of the yield criteria in the numerical simulation of the deep drawing of a cylindrical cup. In: Oñate E, Owen DRJ, editors. COMPLAS-2003. Barcelona; 2003. p. 158.
[64] Alves JL, Menezes LF. Application of tri-linear and tri-quadratic 3D solid FE in sheet metal forming process simulation. In: Mori K, editors. NUMIFORM 2001. Japan; 2001. p. 639–44.
[65] Dougherty JD, Padovan J, Srivatson TS. Fatigue crack propagation and closure behaviour of modified 1071 steel: finite element study. Engng Fract Mech 1997;66(2):189–212.
[66] Haddadi H, Bouvier S, Banu M, Maier C, Teodosiu C. Towards an accurate description of the anisotropic behaviour of sheet metals under large plastic deformations: modelling, numerical analysis and identification. Int J Plasticity 2006;22:2226–71.
[67] Toribio J, Kharin V. Large crack tip deformations and plastic crack advance during fatigue. Mater Lett 2007;61:964–67.
[68] Allison JE, Ku RC, Pompetzki MA. A comparison of measurement methods and numerical procedures for the experimental characterization of fatigue crack closure. ASTM STP 1988;982:171–85.

[69] Schijve J. Some formulas for the crack opening stress level. Engng Fract Mech 1981;14:461–5.
[70] de Koning AU. A simple crack closure model for prediction of fatigue crack growth rates under variable-amplitude loading. ASTM STP 1981;743:63–85.
[71] Newman Jr JC. A crack opening stress equation for fatigue crack growth. Int J Fract 1984;24:R131–5.